J|A|C|S
ARTICLES
Published on Web 10/28/2006

Synthesis of MIL-102, a Chromium Carboxylate Metal−Organic Framework, with Gas Sorption Analysis

Suzy Surblé,[†] Franck Millange,*[,†] Christian Serre,[†] Tina Düren,[‡] Michel Latroche,[§] Sandrine Bourrelly,[⊥] Philip L. Llewellyn,[⊥] and Gérard Férey[∥]

Contribution from the Institut Lavoisier Versailles, UMR 8180, CNRS, Université de Versailles St-Quentin-en-Yvelines, 45 Avenue des Etats-Unis, 78035 Versailles Cedex, France, Institute for Materials and Processes, School of Engineering and Electronics, University of Edinburgh, King's Buildings, Edinburgh EH9 3JL, United Kingdom, Laboratoire de Chimie Métallurgique des Terres Rares, UPR 209, CNRS, 94320 Thiais Cedex, France, and MADIREL, UMR 6121, CNRS, Université de Provence, Centre de St Jérôme, 13397 Marseille Cedex 20, France

Received June 20, 2006; E-mail: millange@chimie.uvsq.fr

Abstract: A new three-dimensional chromium(III) naphthalene tetracarboxylate, $Cr^{III}_3O(H_2O)_2F\{C_{10}H_4(CO_2)_4\}_{1.5}\cdot 6H_2O$ (**MIL-102**), has been synthesized under hydrothermal conditions from an aqueous mixture of $Cr(NO_3)_3\cdot 9H_2O$, naphthalene-1,4,5,8-tetracarboxylic acid, and HF. Its structure, solved ab initio from X-ray powder diffraction data, is built up from the connection of trimers of trivalent chromium octahedra and tetracarboxylate moieties. This creates a three-dimensional structure with an array of small one-dimensional channels filled with free water molecules, which interact through hydrogen bonds with terminal water molecules and oxygen atoms from the carboxylates. Thermogravimetric analysis and X-ray thermodiffractometry indicate that **MIL-102** is stable up to ∼300 °C and shows zeolitic behavior. Due to topological frustration effects, **MIL-102** remains paramagnetic down to 5 K. Finally, **MIL-102** exhibits a hydrogen storage capacity of ∼1.0 wt % at 77 K when loaded at 3.5 MPa (35 bar). The hydrogen uptake is discussed in relation with the structural characteristics and the molecular simulation results. The adsorption behavior of **MIL-102** at 304 K resembles that of small-pore zeolites, such as silicalite. Indeed, the isotherms of CO_2, CH_4, and N_2 show a maximum uptake at 0.5 MPa, with no further significant adsorption up to 3 MPa. Crystal data for **MIL-102**: hexagonal space group $P\bar{6}$ (No. 169), $a = 12.632(1)$ Å, $c = 9.622(1)$ Å.

Introduction

Research activity on metal−organic frameworks is very topical, owing to their interesting magnetic,[1,2] optical,[3,4] gas separation,[5] catalysis,[6] and more recently hydrogen storage properties.[7−9] In this new family of materials, the combination of inorganic clusters, chains, or layers with various organic moieties results in a large variety of open-framework solids showing different pore shapes and dimensions with sometimes unique properties. Under hydrothermal conditions, the study of 3d transition metal carboxylates led to many three-dimensional porous or pillared structures.[10] Most of them are obtained with divalent cations. The most recent references concern manganese,[11,12] iron,[13,14] cobalt,[15−17] nickel,[18−21] copper,[22,23] zinc,[24,25] and cadmium.[12,26] In the field of trivalent metals, results are still scarce and mainly refer to the work of our group on

[†] Université de Versailles St-Quentin-en-Yvelines.
[‡] University of Edinburgh.
[§] Laboratoire de Chimie Métallurgique des Terres Rares.
[⊥] Université de Provence.
[∥] Université de Versailles St-Quentin-en-Yvelines et Institut Universitaire de France.

(1) Maspoch, D.; Ruiz-Molina, D.; Veciana, J. *J. Mater. Chem.* **2004**, *14*, 2713.
(2) Férey, G. *Nat. Mater.* **2003**, *2*, 136.
(3) Serpaggi, F.; Férey, G.; Antic-Fidancev, E. *J. Solid State Chem.* **1999**, *148*, 347.
(4) Millange, F.; Serre, C.; Marrot, J.; Gardant, N.; Pellé, F.; Férey, G. *J. Mater. Chem.* **2004**, *14*, 642.
(5) Rosseinsky, M. J. *Microporous Mesoporous Mater.* **2004**, *73*, 15.
(6) Seo, J. S.; Whang, D.; Lee, H.; Jun, S. I.; Oh, J.; Jeon, Y. J.; Kim, K. *Nature* **2000**, *404*, 982.
(7) Férey, G.; Latroche, M.; Serre, C.; Millange, F.; Loiseau, T.; Percheron-Guégan, A. *Chem. Commun.* **2003**, 2976.
(8) Rosi, N. L.; Eckert, J.; Eddaoudi, M.; Vodak, D. T.; Kim, J.; O'Keeffe, M.; Yaghi, O. M. *Science* **2003**, *300*, 1127.
(9) Rowsell, J. L. C.; Millward, A. R.; Park, K. S.; Yaghi, O. M. *J. Am. Chem. Soc.* **2004**, *126*, 5666.
(10) Rao, C. N. R.; Natarajan, S.; Vaidhyanathan, R. *Angew. Chem., Int. Ed.* **2004**, *43*, 1466.
(11) Li, L. J.; Li, Y. *J. Mol. Struct.* **2004**, *694*, 199.
(12) Zheng, Y. Q.; Sun, D. *J. Solid State Chem.* **2003**, *172*, 288.
(13) Sanselme, M.; Grenèche, J. M.; Riou-Cavellec, M.; Férey, G. *Chem. Commun.* **2002**, 2172.
(14) Riou-Cavellec, M.; Lesaint, C.; Nogues, M.; Grenèche, J. M.; Férey, G. *Inorg. Chem.* **2003**, *42*, 5669.
(15) Livage, C.; Egger, C.; Férey, G. *Chem. Mater.* **2001**, *13*, 410.
(16) Livage, C.; Guillou, N.; Marrot, J.; Férey, G. *Chem. Mater.* **2001**, *13*, 4387.
(17) Huang, Z.-L.; Drillon, M.; Masciocchi, N.; Sironi, A.; Zhao, J.-T.; Rabu, P.; Panissod, P. *Chem. Mater.* **2000**, *12*, 2805.
(18) Fletcher, A. J.; Cussen, E. J.; Bradshaw, D.; Rosseinsky, M. J.; Thomas, K. M. *J. Am. Chem. Soc.* **2004**, *126*, 9750.
(19) Forster, P. M.; Cheetham, A. K. *Angew. Chem., Int. Ed.* **2002**, *41*, 457.
(20) Guillou, N.; Livage, C.; van Beek, W.; Nogues, M.; Férey, G. *Angew. Chem., Int. Ed.* **2003**, *42*, 644.
(21) Guillou, N.; Livage, C.; Drillon, M.; Férey, G. *Angew. Chem., Int. Ed.* **2003**, *42*, 5314.
(22) Chui, S. S. Y.; Lo, S. M. F.; Charmant, J. P. H.; Orpen, A. G.; Williams, I. D. *Science* **1999**, *283*, 1148.
(23) Forster, P. M.; Thomas, P. M.; Cheetham, A. K. *Chem. Mater.* **2002**, *14*, 17.
(24) Rowsell, J. L. C.; Yaghi, O. M. *Microporous Mesoporous Mater.* **2004**, *73*, 3.
(25) Erxleben, A. *Coord. Chem. Rev.* **2003**, *246*, 203.
(26) Sun, J.; Zheng, Y. Q. *Z. Anorg. Allg. Chem.* **2003**, *629*, 1001.

vanadium[27−29] and chromium[30,31] for their magnetic applications and as well as work on indium,[32] while many rare earth materials have been studied for their luminescence properties.[4,33] Both the usual serendipity inherent to this emerging field and the new rational structural prediction that we recently introduced[34,35] are expected to bring about a rapid increase in the number of candidates. Our new rational approach concerns the determination of the chemical conditions of synthesis associated with the existence of the inorganic oligomer which participates in the structure. First applied to trimers of μ_3-oxo-linked octahedra under hydrothermal conditions, this approach led to the first open-framework iron(III) carboxylates[35,36] and then to giant-pore chromium(III) carboxylates **MIL-100** and **MIL-101**, which exhibit a giant cell, a zeotype architecture, and a hierarchy of micro- and mesopores.[37,38]

The demand for an efficient and clean fuel alternative has increased in recent years and is expected to become more pronounced in the future. Hydrogen is considered one of the best alternative fuels[39] due its abundance, easy synthesis, and nonpolluting nature when used in fuel cells.[40] Hydrogen may be stored in solids by two principal mechanisms: (i) chemisorption, where hydrogen atoms may be dissolved or form chemical bonds, and (ii) physisorption, where hydrogen molecules adsorb onto surfaces. Among the various candidates for storage, including porous sorbents, reversible metal hydrides, chemical hydrides, compressed gas, and liquefaction, none is capable of meeting the U.S. Department of Energy cost and performance targets.[41] Recently, a new class of crystalline material that possesses a very low density and high surface area, the so-called metal−organic frameworks (MOFs) and similar porous materials, have shown hydrogen storage capacities.[7−9,42−48] Adsorption of H_2 molecules in MOFs seems to be a promising solution. For example, Wong-Foy et al. reported hydrogen storage capacities of up to 7.5 wt % at 77 K and 60 bar.[49] Several MOFs and related porous materials have shown considerable hydrogen uptake at 77 K,[7−9,42−53] and MOFs seem to be a viable option for hydrogen storage. Owing to the chemical richness of this family, the challenge of finding promising materials becomes immense, and the number of papers on this topic is increasing steadily, describing tests on known phases as well as the search for new "efficient" solids by analyzing the factors that influence hydrogen storage. MOF-type materials in general show promising properties for gas adsorption. Indeed, they could be of interest in relation to one of the technological problems that faces society today: the environmentally friendly and economically favorable separation, capture, and storage of gases. This is especially the case for carbon dioxide and will be critically important in Europe, moving toward an H_2-based economy. It is thus important to find a new way to capture and store CO_2 produced during various industrial processes under different conditions. In processes such as pressure swing adsorption for the capture of CO_2, adsorbents such as zeolites are adequate but difficult to regenerate without significant heating, entailing low productivity and high costs. MOF materials can be regenerated under milder conditions than most zeolites. Such MOF materials are thus promising alternative solids for these applications.

In this context, we describe here the synthesis, structure determination, and sorption properties (H_2, CO_2, CH_4, and N_2) of the metal−naphthalene-1,4,5,8-tetracarboxylate complex $Cr^{III}_3O(H_2O)_2F\{C_{10}H_4(CO_2)_4\}_{1.5}\cdot 6H_2O$, containing trivalent chromium, hereafter denoted **MIL-102**.

Experimental Section

Synthesis. MIL-102 was synthesized hydrothermally (autogenous pressure) from a mixture of chromium(III) nitrate ($Cr(NO_3)_3\cdot 9H_2O$, 400 mg, 1 mmol; Aldrich, 99%), naphthalene-1,4,5,8-tetracarboxylic acid ($C_{10}H_4(CO_2H)_4$, 203 mg, 0.66 mmol; Sigma Aldrich, 97%), hydrofluoric acid (2 mmol), and H_2O in the molar ratio 1:0.66:2:255. Reactants were introduced in this order and stirred for approximately 10 min before the resulting mixture was placed in a Teflon-lined steel autoclave. The mixture was held at 200 °C for 15 h. The pH remained acidic (∼1) during the course of the synthesis. A laboratory powder X-ray diffraction pattern of the green solid product, after it was recovered and washed with water, showed that a novel crystalline phase had been produced, although it was contaminated with a small amount of unreacted naphthalene-1,4,5,8-tetracarboxylic acid. The green product was scrubbed in *N*,*N*-dimethylformamide at room temperature to remove traces of the unreacted acid. It has not been possible to prepare crystals of suitable size for single-crystal diffraction studies; for example, if the reaction mixture stood for longer periods, no change in the sample nature was observed, and seeding the mixture with pre-made sample afforded no larger crystals.

Elemental Analysis. MIL-102 elemental analysis gave the following results: Cr, 18.6%; C, 31.4%; F, 1.7%; H, 2.7%. These values compare well with those calculated from the proposed formula, $Cr^{III}_3O(H_2O)_2F\{C_{10}H_4(CO_2)_4\}_{1.5}\cdot 6H_2O$: Cr, 19.9%; C, 32.1%; F, 2.4%; H, 2.8%.

Density Measurement. The bulk density measurement was performed with a Micromeretics Accupyc 1330 apparatus using helium gas. The observed result (2.0(1) $g\cdot cm^{-3}$) is in good agreement with the one calculated on the basis of the structural formula (1.96 $g\cdot cm^{-3}$).

Thermogravimetry. Thermogravimetric analysis was carried out

(27) Barthelet, K.; Marrot, J.; Riou, D.; Férey, G. *Angew. Chem., Int. Ed.* **2002**, *41*, 281.
(28) Barthelet, K.; Adil, K.; Millange, F.; Serre, C.; Riou, D.; Férey, G. *J. Mater. Chem.* **2003**, *13*, 2208.
(29) Barthelet, K.; Marrot, J.; Férey, G.; Riou, D. *Chem. Commun.* **2004**, 520.
(30) Millange, F.; Serre, C.; Férey, G. *Chem. Commun.* **2002**, 822.
(31) Serre, C.; Millange, F.; Thouvenot, C.; Nogues, M.; Marsolier, G.; Louër, D.; Férey, G. *J. Am. Chem. Soc.* **2002**, *124*, 13519.
(32) Gomez-Lor, B.; Gutierrez-Puebla, E.; Iglesias, M.; Monge, M. A.; Ruiz-Valero, C.; Snejko, N. *Inorg. Chem.* **2002**, *41*, 2429.
(33) Serre, C.; Pellé, F.; Gardant, N.; Férey, G. *Chem. Mater.* **2004**, *16*, 1177.
(34) Mellot-Draznieks, C.; Dutour, J.; Férey, G. *Angew. Chem., Int. Ed.* **2004**, *43*, 6290.
(35) Serre, C.; Millange, F.; Surblé, S.; Férey, G. *Angew. Chem., Int. Ed.* **2004**, *43*, 6286.
(36) Serre, C.; Millange, F.; Surblé, S.; Férey, G. *Chem. Mater.* **2004**, *16*, 2706.
(37) Férey, G.; Serre, C.; Mellot-Draznieks, C.; Millange, F.; Surblé, S.; Dutour, J.; Margiolaki, I. *Angew. Chem., Int. Ed.* **2004**, *43*, 6296.
(38) Férey, G.; Mellot-Draznieks, C.; Serre, C.; Millange, F.; Dutour, J.; Surblé, S.; Margiolaki, I. *Science* **2005**, *309*, 2040.
(39) Dell, R. M.; Rand, D. A. J. *J. Power Sources* **2001**, *100*, 2.
(40) McNicol, B. D.; Rand, D. A. J.; Williams, K. R. *J. Power Sources* **2001**, *100*, 47.
(41) http://www.eere.energy.gov/hydrogenandfuelcells/storage/storage_challenges.html
(42) Dybtsev, D. N.; Chun, H.; Kim, K. *Angew. Chem., Int. Ed.* **2004**, *43*, 5033.
(43) Dybtsev, D. N.; Chun, H.; Yoon, S. H.; Kim, D.; Kim, K. *J. Am. Chem. Soc.* **2004**, *126*, 32.
(44) Kesanli, B.; Cui, Y.; Smith, M. R.; Bittner, E. W.; Bockrath, B. C.; Lin, W. B. *Angew. Chem., Int. Ed.* **2005**, *44*, 72.
(45) Zhao, X. B.; Xiao, B.; Fletcher, A. J.; Thomas, K. M.; Bradshaw, D.; Rosseinsky, M. J. *Science* **2004**, *306*, 1012.
(46) Pan, L.; Sander, M. B.; Huang, X.; Li, J.; Smith, M.; Bittner, E.; Bockrath, B.; Johnson, J. K. *J. Am. Chem. Soc.* **2004**, *126*, 1308.
(47) Lee, E. Y.; Suh, M. P. *Angew. Chem., Int. Ed.* **2004**, *43*, 2798.
(48) Panella, B.; Hirscher, M. *Adv. Mater.* **2005**, *17*, 538.
(49) Wong-Foy, A. G.; Matzger, A. J.; Yaghi, O. M. *J. Am. Chem. Soc.* **2006**, *128*, 3494.
(50) Sun, D. F.; Ma, S. Q.; Ke, Y. X.; Collins, D. J.; Zhou, H. C. *J. Am. Chem. Soc.* **2006**, *128*, 3896.
(51) Rowsell, J. L. C.; Yaghi, O. M. *J. Am. Chem. Soc.* **2006**, *128*, 1304.
(52) Panella, B.; Hirscher, M.; Putter, H.; Muller, U. *Adv. Funct. Mater.* **2006**, *16*, 520.
(53) Mueller, U.; Schubert, M.; Teich, F.; Puetter, H.; Schierle-Arndt, K.; Pastre, J. *J. Mater. Chem.* **2006**, *16*, 626.

on a TGA type 2050 thermogravimetric analyzer under a flow of oxygen gas at a heating rate of 2 °C min^{-1} from 20 to 600 °C.

Infrared Spectroscopy. Infrared spectroscopy, performed with a Nicolet Magma 550 IR apparatus, indicates the presence of vibrational bands characteristic of the organic moieties, with the −(O−C−O)− bands around 1620 and 1450 cm^{-1} confirming the presence of the tetracarboxylate moieties within the solid. A large band around 3480 cm^{-1} also confirmed the presence of H_2O molecules.

Powder X-ray Diffraction. Two powder X-ray diffraction methods were used to characterize the solid.

Temperature-dependent X-ray powder diffraction measurements were performed using a Siemens D5000 diffractometer ($\theta-\theta$ mode, Co Kα radiation, $\lambda = 1.7903$ Å) equipped with an Anton Paar HTK16 high-temperature device and an M Braun linear position-sensitive detector (PSD) under static air. Patterns were scanned with a resolution of 0.0147° and a divergence slit of 0.1° over the angular range $2\theta = 8-30°$ to observe the most intense low-angle Bragg reflections. Temperature steps of 10 °C from 20 to 600 °C were typically used.

Ambient X-ray powder diffraction data on the new compound were collected on a Bruker D8 Advance AXS diffractometer ($\theta-2\theta$ mode, Cu Kα radiation, $\lambda = 1.5406$ Å). The powder diffraction pattern was scanned over the angular range $2\theta = 5-80°$ with a step size of 0.02°.

Sorption Experiments. (i) Experiments at 77 K. The specific surface area was measured on the sample activated for 15 h at 200 °C, with a Micrometrics ASAP 2010 apparatus using nitrogen as the adsorbed gas. For the hydrogenation measurements, about 0.5 g of powder was transferred in an air-tight stainless steel sample holder connected to a volumetric device equipped with pressure gauges to measure the hydrogen amount loaded (or unloaded) from the sample. Before measurement of the sorption properties, outgassing of the samples was performed overnight at 220 °C under primary vacuum for dehydration. Thus, all data given here refer to mass capacity for dehydrated materials. Adsorption curves were recorded step-by-step from pressure variation measurements in calibrated and thermalized gauged volumes (Sievert's method). For measurements at 77 K, the sample holder was immersed in liquid nitrogen, and the pressure variations due to both gas cooling and hydrogen adsorption were measured. Under these thermodynamic conditions ($0 < P < 10$ MPa; $77 < T < 298$ K), the ideal gas law is no longer valid, and different equations of state were used, depending on the temperature range.[54,55]

(ii) Experiments at 304 K. Prior to each adsorption experiment, the sample was outgassed using sample controlled thermal analysis.[56] These conditions maintained a constant residual vacuum pressure of 2 Pa up to a final temperature of 450 °C, which was kept until the residual pressure dropped below 5×10^{-3} mbar. The adsorption at 304 K up to 3 MPa was carried out by means of a manometric device built in-house. Doses of gas were successively introduced up to a final pressure of 3 MPa. The reported experimental data correspond to adsorption values obtained from the correction of the primary excess values via the following expression:

$$n^{a} = n^{\sigma} + \frac{PV^{zeo}}{RT}$$

where n^{a} and n^{σ} are the absolute and excess amounts adsorbed, respectively, and V^{zeo} is the micropore volume of the various samples, estimated from nitrogen physisorption at 77 K. Moreover, for such studies at ambient temperature and high pressure, an appropriate expression for gas non-ideality was included using the Gasem−Peng−Robinson equation of state.

Magnetic Measurements. Experiments were performed on a powder sample of **MIL-102** over the temperature range of 5−300 K, with a SQUID magnetometer for an external applied magnetic field B of 0.1 T. The samples were first zero-field-cooled, and the magnetic field was applied after stabilization of the temperature at 4.5 K. Raw data were corrected for the sample holder contribution and the core diamagnetism.

Simulations. Adsorption isotherms were simulated with grand canonical Monte Carlo (GCMC) simulations using the multipurpose simulation code MUSIC.[57] Atomistic models were employed for both the sorbate molecules and the **MIL-102** framework. As the position of the fluorine atoms in the framework is disordered, different positions were tested, but position was found to have negligible influence. All results reported here were obtained with fluorine in the para position. The interatomic interactions were modeled with the Lennard-Jones potential, with potential parameters for the framework taken from the UFF force field[58] and parameters for the hydrogen molecule from Yang and Zhong.[59] Lennard-Jones interactions beyond 12.8 Å and electrostatic interactions were neglected. The simulations were equilibrated for one million steps, and a further one million steps were used to sample the data. The absolute number of molecules, i.e., the simulation result, is converted to the excess number of molecules, i.e., the experimentally measured quantity, as described by Myers and Monson.[60] The isosteric heat of adsorption was calculated according to ref 61. For all thermodynamic calculations, the Peng−Robinson equation of state was used.

Results and Discussion

Structure Solution. Since no single crystals suitable for analysis were obtained, an ab initio structure determination based on the powder diffraction analysis was carried out. Determination of the peak positions for the Cu Kα radiation contribution was carried out by means of the Winplotr program.[62] Pattern indexing was then performed by means of the computer program DICVOL91[63] from the first 20 lines, with an absolute error in peak positions of 0.03° (2θ). Satisfactory figures of merit[64,65] (see Table 1) were thus obtained. **MIL-102** crystallizes with a primitive hexagonal cell [$a = 12.632(1)$ Å and $c = 9.622(1)$ Å]. A structureless whole pattern profile refinement by the Le Bail[66] method, using the program Fullprof,[67] confirmed the adequacy of the cell. Structure determination was performed using the EXPO[68] package, which combines the full pattern decomposition program EXTRA[69] and the direct methods program SIR97,[68] optimized for powder diffraction data. The centric $P\bar{6}$ (No. 169) space group was chosen to solve the structure. The first electron density map revealed the localization of almost all the atoms of the inorganic skeleton. The overall character of the structure was clearly defined. The distance between the three nearest chromium atoms was found to be $d_{Cr-Cr} = 3.25-3.50$ Å, which is very similar to those encountered in "trimers of μ_3-oxo-linked octahedra-like" phases: d_{Cr-Cr}

(54) Younglove, B. A. *J. Phys. Chem. Ref. Data* **1982**, *11*, 353.
(55) Hemmes, H.; Driessen, A.; Griessen, R. *J. Phys. C: Solid State Phys.* **1986**, *19*, 3571.
(56) Rouquerol, J. *Thermochim. Acta* **1989**, *144*, 209.
(57) Gupta, A.; Chempath, S.; Sanborn, M. J.; Clark, L. A.; Snurr, R. Q. *Mol. Simul.* **2003**, *29*, 29.
(58) Rappe, A. K.; Casewit, C. J.; Colwell, K. S.; Goddard, W. A.; Skiff, W. M. *J. Am. Chem. Soc.* **1992**, *114*, 10024.
(59) Yang, Q. Y.; Zhong, C. L. *J. Phys. Chem. B* **2005**, *109*, 11862.
(60) Myers, A. L.; Monson, P. A. *Langmuir* **2002**, *18*, 10261.
(61) Heuchel, M.; Snurr, R. Q.; Buss, E. *Langmuir* **1997**, *13*, 6795.
(62) Roisnel, T.; Rodriguez-Carvajal, J. *Abstracts of the 7th European Powder Diffraction Conference*; Barcelona, Spain, 2000; p 71.
(63) Boultif, A.; Louër, D. *J. Appl. Crystallogr.* **1991**, *24*, 987.
(64) de Wolff, P. M. *J. Appl. Crystallogr.* **1972**, *5*, 243.
(65) Smith, G. S.; Snyder, R. L. *J. Appl. Crystallogr.* **1979**, *12*, 60.
(66) Le Bail, A.; Duroy, H.; Fourquet, J. *Mater. Res. Bull.* **1988**, *23*, 447.
(67) Rodriguez-Carvajal, J. *Collected Abstracts of Powder Diffraction Meeting*; Toulouse, France, 1990; p 127.
(68) Altomare, A.; Burla, M. C.; Camalli, M.; Carrozzini, B.; Cascarano, G. L.; Giacovazzo, C.; Guagliardi, A.; Moliterni, A. G. G.; Polidori, G.; Rizzi, R. *J. Appl. Crystallogr.* **1999**, *32*, 339.
(69) Altomare, A.; Burla, M. C.; Cascarano, G. L.; Giacovazzo, C.; Guagliardi, A.; Moliterni, A. G. G.; Polidori, G. *J. Appl. Crystallogr.* **1995**, *28*, 842.

Table 1. Crystal Data and Structure Refinement Parameters for **MIL-102**[a]

formula	$Cr^{III}_6O_2\{H_2O\}_4{\cdot}F_2{\cdot}\{C_{10}H_4(CO_2)_4\}_3{\cdot}12H_2O$
formula weight ($g{\cdot}mol^{-1}$)	1570.76
calcd density ($g{\cdot}cm^{-3}$)	1.96
crystal system	hexagonal
space group	$P\bar{6}$ (No. 169)
a (Å)	12.632(1)
c (Å)	9.622(1)
V (Å^3)	1329.7(2)
figures of merit	$M_{20} = 100$; $F_{20} = 158$ (0.0042, 30)
Z	1
radiation (Cu Kα_1), λ (Å)	1.5406
2θ range (°)	5−80
no. of reflections	352
no. of atoms	20
no. of intensity-dependent parameters	51
no. of profile parameters	10
R_P	0.093
R_{WP}	0.120
R_B	0.071
R_F	0.080

[a] Overall thermal parameter, 2.0 Å.^{2}

= 3.26 Å for (μ_3-oxo)hexakis(μ_2-acetato)triaquatrichromium-(III) 2,6-dihydroxybenzoate dihydrate.[70] By analogy, it was assumed that, as a starting point for construction of a structural model, **MIL-102** should contain these trimeric inorganic species (three metallic octahedra shared by a μ_3-oxo atom). The corresponding atomic coordinates were used as a starting model in the Rietveld refinement. The pseudo-Voigt function and the usual quadratic function in tan θ were used to describe the individual line profile and the angular dependence of the peak full width at half-maximum, respectively. The use of soft distance and angular constaints to regularize the starting structural model gave a slightly clearer difference electron density map. Further alternate cycles of refinement and successive difference Fourier maps using SHELXL[71] allowed complete location of organic moieties and the occluded water molecules (according to the TGA measurement). The final Rietveld refinement was carried out over the angular range of 5−80° (2θ) by using 352 reflections. Details of the refinement are summarized in Table 1, final non-hydrogen atomic parameters are given in Table 2, and selected bond distances are listed in Table 3. The final Rietveld plot is given in Figure 1.

Structure Description. The X-ray structure determinations reveal that the structures of **MIL-102** contain trimers of chromium(III) octahedra linked through tetracarboxylate anions, creating a three-dimensional framework (Figure 2). There are two crystallographically independent chromium atoms, Cr1 and Cr2, and each chromium atom exhibits an octahedral environment with four oxygen atoms from the bidentate carboxylates, one μ_3-oxo atom, and one terminal site. The latter site can be occupied by a terminal water molecule and/or a fluorine anion, leading to the formation of a trimeric chromium subunit. At this stage, using powder data diffraction, it was not possible to distinguish between the water molecule and the fluorine anion. However, recent infrared spectroscopy measurements performed on the **MIL-100**[37] compound (which exhibits the same trimeric chromium subunit and the same fluorine content, F/Cr = 1:3) have shown that the three terminal sites (one per chromium atom of the trimer) are occupied by fluorine and water molecules in a 1:2 ratio.[72] So, the trimeric chromium subunit must be labeled $\{Cr^{III}_3O(H_2O)_2F\}^{6+}$. The same behavior is expected in the case of **MIL-102**, and the formula deduced from the structure determination is then $Cr^{III}_3O(H_2O)_2F\{C_{10}H_4(CO_2)_4\}_{1.5}{\cdot}6H_2O$.

Along [001], each trimer is connected to its equivalent by the bridging carboxylate functions of the organic moiety. If one

Table 2. Atomic Coordinates for **MIL-102**

atom	*x/a*	*y/b*	*z/c*
Cr1	0.044(1)	0.165(1)	0
Cr2	0.538(1)	0.385(1)	0
μ_3-O1	0	0	0
μ_3-O2	2/3	1/3	0
O3	0.502(2)	0.098(2)	0.852(2)
O4	−0.053(1)	0.175(1)	0.849(1)
O5	−0.205(2)	−0.020(1)	0.863(2)
O6	0.479(5)	0.265(1)	0.181(2)
O7w or (F7)	0.115(3)	0.347(2)	0
O8w or (F8)	0.398(2)	0.411(2)	0
C1	−0.155(2)	0.084(1)	0.795(1)
C2	−0.171(2)	0.085(1)	0.649(1)
C3	−0.203(2)	−0.020(1)	0.567(1)
C4	−0.145(3)	0.192(1)	0.575(1)
C5	−0.105(2)	0.311(1)	0.658(1)
C6	0.475(2)	0.168(2)	0.779(1)
C7	−0.078(2)	0.412(1)	0.571(1)
Ow1	0.522(2)	0.754(2)	0.270(1)
Ow2	−0.535(2)	−0.199(2)	1/2
Ow3	0.182(2)	0.561(2)	0

Table 3. Principal Bond Lengths (Å) for **MIL-102**

Cr1−μ_3-O1	1.87(1)	Cr2−μ_3-O2	2.02(2)
Cr1−O4	1.95(2)	Cr2−O3	1.89(2)
Cr1−O4	1.95(2)	Cr2−O3	1.89(2)
Cr1−O5	2.06(2)	Cr2−O6	2.18(2)
Cr1−O5	2.06(2)	Cr2−O6	2.18(2)
Cr1−O7w or (F7)	2.00(2)	Cr2-O8w or (F8)	1.96(3)
C1−O4	1.33(2)	C6−O3	1.30(3)
C1−O5	1.31(2)	C6−O6	1.26(3)
C1−C2	1.41(1)	C4−C5	1.54(1)
C2−C4	1.41(2)	C5−C6	1.40(3)
C2−C3	1.42(2)	C5−C7	1.42(2)
C3−C3	1.29(2)	C7−C7	1.36(1)
C4−C4	1.45(1)		

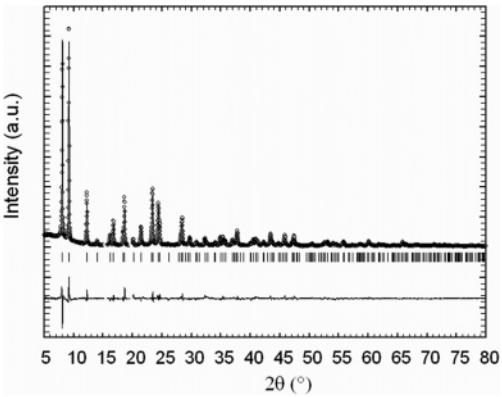

Figure 1. Final Rietveld plot of **MIL-102**. Observed, calculated, and difference profiles are plotted on the same scale. Bragg peaks are indicated by tic marks.

(70) Glowiak, T.; Koslowski, H.; Erre, L. S.; Micera, G. *Inorg. Chim. Acta* **1996**, *248*, 99.
(71) Sheldrick, G. M. *SHELXL*; University of Göttingen: Göttingen, Germany, 1997.
(72) Vimont, A.; Goupil, J. M.; Lavalley, J. C.; Daturi, M.; Surblé, S.; Serre, C.; Millange, F.; Férey, G.; Audebrand, N. *J. Am. Chem. Soc.* **2006**, *128*, 3218.

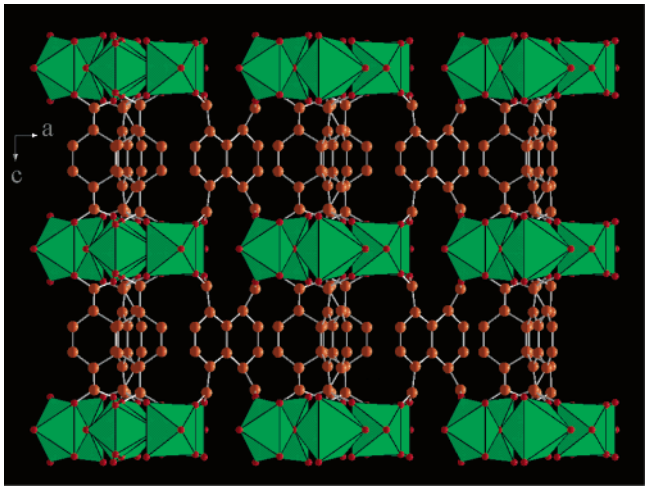

Figure 2. Polyhedral view of the structure of **MIL-102** along the *b*-axis. Green polyhedra are chromium octahedra; large circles (red and orange) are oxygen and carbon atoms, respectively.

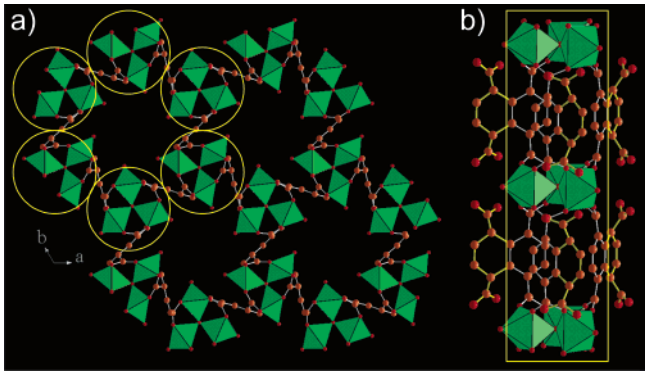

Figure 3. (a) View of the structure of **MIL-102** along the *c*-axis, described in terms of juxtaposition of "bamboo" nanotubes (represented by circles). Green polyhedra are chromium octahedra; large circles (red and orange) are oxygen and carbon atoms, respectively. (b) Perspective view of one nanotube. The connection between nanotubes is ensured by the naphthalene rings. Half of each naphthalene-1,4,5,8-tetracarboxylate moiety belongs to one nanotube.

considers that the naphthalene-1,4,5,8-tetracarboxylate moiety could be described as resulting from the fusion of two 1,4-benzenedicarboxylate moieties (even if the two sets are chemically different entities, aside from their structural similarity), an alternative description of the structure can be proposed. It is based on the existence of "bamboo" rods. If these rods were built up from 1,4-benzenedicarboxylates, the benzene rings would be in the plane formed by the O−C−O groups. In **MIL-102**, these rings are rotated by 30°, because they belong to naphthalene groups, which ensures the connection between two rods (Figure 3a). The advantage of this description is that it highlights the existence of a special kind of nanotube which shares the central C−C bond of the naphthalene groups (Figure 3b). The hexagonal arrangement of such nanotubes, which is also reminiscent of hexagonal mesophases, creates one-dimensional pore channels along the *c*-axis, where six free water molecules are located. Their free diameter (i.e., with the van der Waals radius substracted) is ∼4.4 Å. It is also clear from Figure 3a that the terminal water molecules or fluorine anions point toward the center of the tunnels. Distances and angles are, on the whole, well defined (see Table 3). Bond valence calculations[73] lead to values of 3.0(1) and 2.9(1) for the chromium atoms for **MIL-102**.

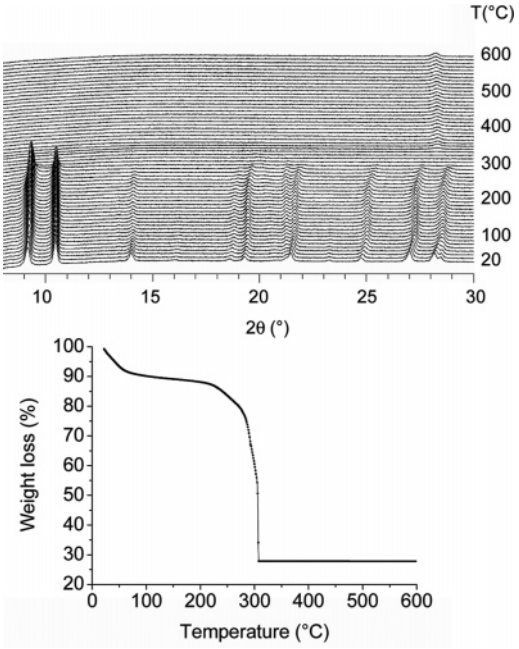

Figure 4. (Top) X-ray thermodiffractogram of **MIL-102** under air atmosphere. (Bottom) TGA under air atmosphere.

MIL-102 is a new example of a trivalent 3d metal carboxylate built up from trimeric building units. The previously described solids, labeled **MIL-59** (vanadium isophthalate),[74] **MIL-88** (iron fumarate),[35,75] **MIL-89** (iron muconate),[35] **MIL-100** (chromium trimesate),[37] and **MIL-101** (chromium terephthalate),[38] used di- or tricarboxylates. Thus, **MIL-102** is the first solid of this series built up from tetracarboxylate groups. From chemical and mechanistic points of view, this shows that the in situ generation of trimeric inorganic subunits under solvo- or hydrothermal conditions depends only on the nature of the metallic precursor and on the chemical conditions (pH, concentrations, etc.) but not on the size and the shape of the organic linker.

Thermal Properties. The thermal stability of **MIL-102** was examined by thermogravimetry analysis (TGA) and variable-temperature powder X-ray diffraction (HTXRD). The TG curves exhibit three significant mass changes over the temperature ranges 25−100, 225−265, and 265−300 °C (Figure 4, bottom). Thermogravimetric analyses are in agreement with the formulation of $Cr^{III}_3O(H_2O)_2F\{C_{10}H_4(CO_2)_4\}_{1.5}\cdot 6H_2O$. A first weight loss of 11.9% occurs below 100 °C and corresponds to the loss of occluded water in the structure (expected weight loss 13.8%). The corresponding formula of the sample at this stage is $Cr^{III}_3O(H_2O)_2F\{C_{10}H_4(CO_2)_4\}_{1.5}$. The departure of the terminal water molecules occurs between 225 and 265 °C (second weight loss of 5.2%, expected 4.6%), in agreement with the formulation of $Cr^{III}_3OF\{C_{10}H_4(CO_2)_4\}_{1.5}$. The removal of the organic moieties and the fluorine anion (weight loss of 53.9%) leads to the destruction of the structure and the formation of chromium oxide, Cr_2O_3 (expected weight loss 52.6%). The determination of crystalline phases formed during calcinations at various temperatures is useful for assessing the thermal stability of the material. A general view (Figure 4, top) shows the whole HTXRD plot of **MIL-102**. First, variable-temperature powder

(73) Brese, N. E.; O'Keeffe, M. *Acta Crystallogr.* **1991**, *B47*, 192.
(74) Barthelet, K.; Riou, D.; Férey, G. *Chem. Commun.* **2002**, 1492.
(75) Surblé, S.; Serre, C.; Mellot-Draznieks, C.; Millange, F.; Férey, G. A. *Chem. Commun.* **2006**, 284.

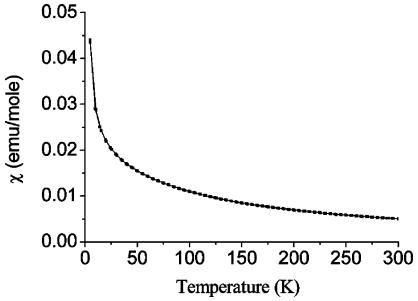

Figure 5. Susceptibility measurement versus temperature of **MIL-102**.

X-ray diffraction studies show that **MIL-102** is stable up to ~300 °C and crystallinity is retained upon the loss of water. It is also clear that the departure of water molecules is not followed by a significant contraction of the pores, confirming that **MIL-102** exhibits a rigid framework, probably due to the existence of the four carboxylate functions around the rigid naphthalene ring. It should be noted that **MIL-102** rehydrates in a short period of time (a few minutes) after dehydration at 200 °C, with no loss of crystallinity, confirming its zeolitic character. At higher temperatures, the departure of the organic moieties leads to the destruction of the framework, and the resulting amorphous phase crystallizes at higher temperatures to give Cr_2O_3. The thermal behavior of **MIL-102** can be summarized through the following scheme:

$$Cr_3O\{H_2O\}_2F\{C_{10}H_4(CO_2)_4\}_{1.5}\cdot 6H_2O \xrightarrow{T < 200\ ^\circ C} Cr_3O\{H_2O\}_2F\{C_{10}H_4(CO_2)_4\}_{1.5} \xrightarrow{T < 265\ ^\circ C} Cr_3OF\{C_{10}H_4(CO_2)_4\}_{1.5} \xrightarrow{T > 300\ ^\circ C} \text{amorphous} \xrightarrow{T > 400\ ^\circ C} Cr_2O_3$$

Magnetic Properties. In the whole temperature range investigated, **MIL-102** is paramagnetic (Figure 5). The inverse molar susceptibility curve, $1/\chi_{dc}$, follows a Curie−Weiss law, $\chi_{dc} = C/(T - \theta_p)$, with $\theta_p = -70$ K indicative of antiferromagnetic interactions at very low temperatures ($T_N < 5$ K) and an experimental effective moment, $\mu_{eff} = 3.87\ \mu_B$, deduced from the Curie constant in perfect agreement with its theoretical value ($\mu_{eff} = g[S(S+1)]^{1/2}$, with $g = 2$ and $S = {}^3/_2$). One can note that the large value of $|\theta_p/T_N|$ suggests the presence of highly frustrated antiferromagnetic interactions, in agreement with the triangular shape and the 120° superexchange angles between the Cr^{3+} polyhedra in the trimer. This highly frustrated character explains the absence of three-dimensional order in the title compound.

Sorption Properties. Nitrogen sorption was first tested at 77 K on a freshly out-gassed sample of **MIL-102**, activated overnight at 200 °C under primary vacuum. It shows a very small gas uptake with a Langmuir area of 42.1(7) m^2/g, coherent with the small free diameter of the tunnels. In a second step, the hydrogen gas uptake by **MIL-102** was measured at 77 K on out-gassed samples (15 h at 220 °C under primary vacuum). **MIL-102** shows a capacity of ~1.0 wt % at 3.5 MPa (Figure 6). It should be noted that, at 77 K, the uptake of this material is lower than that of other MOFs under much less pressure.[7−9,42−48] At room temperature, a very small adsorption (~0.05 wt % at 35 bar) has been measured. Both simulation and experiment suggest that the uptake at room temperature is very small, but there is definitely some uptake (see below).

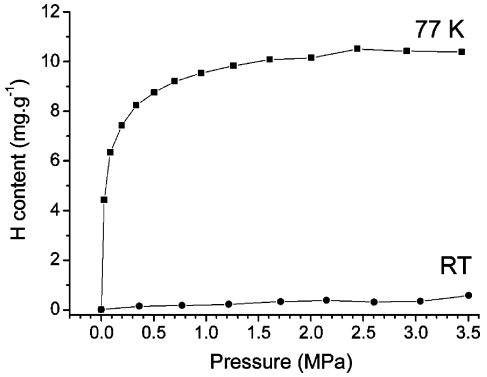

Figure 6. Hydrogen adsorption isotherms at 77 K (top) and room temperature (bottom).

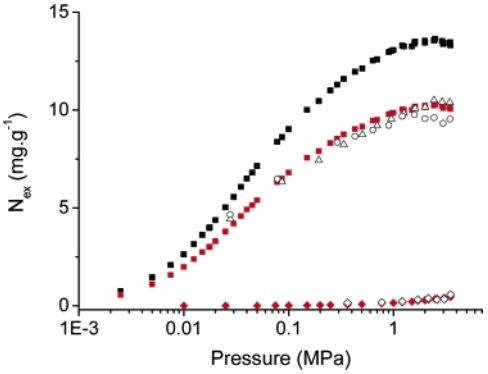

Figure 7. Comparison between experimentally measured (open symbols) and simulated (closed symbols) adsorption isotherms of hydrogen in **MIL-102** at different temperatures (■, 77 K; ◆, 298 K). The black symbols represent the results in a perfect crystal, the red symbols the scaled results in order to take into account defects that are present in the real material.

The GCMC simulations were carried out in a perfect crystal and therefore overpredict the maximum amount (of hydrogen) adsorbed by about one-third at 77 K, as illustrated in Figure 7. Taking into account that the real material has nonporous defects and inaccessible pores, a scaling factor, the ratio of the experimental and the simulated maximum amounts adsorbed ($\Phi = 0.76$), was applied to the simulation data. Note that this scaling factor corresponds to the ratio of the experimental pore volume (0.12 cm^3/g) to the theoretical pore volume (0.158 cm^3/g) and is therefore a measure of how much of the theoretical pore volume is accessible in the material used in the experiments. The difference between the theoretical and the experimental values is due to solvent molecules and probably unreacted reactant left in the pore after activation and imperfections of the crystals. The log plot in Figure 7 shows that the experimental and simulated isotherms agree. In particular, the S-shape of the isotherm, typical for a microporous material, is reproduced very well over the whole pressure range, which is an important benchmark for the quality of the simulation results. The simulations also reproduce the data at 298 K. Furthermore, molecular simulations provide detailed information about the energetic interaction. The simulated heat of adsorption as a function of the amount adsorbed is presented in Figure 8. It is nearly independent of the loading, exhibiting only a slight maximum, which is an indication of an energetically homogeneous material. (For an energetically heterogeneous adsorbent,

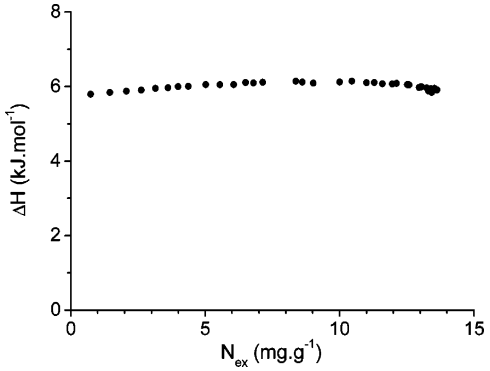

Figure 8. Simulated isosteric heat of adsorption, ΔH, as a function of the amount adsorbed at 77 K.

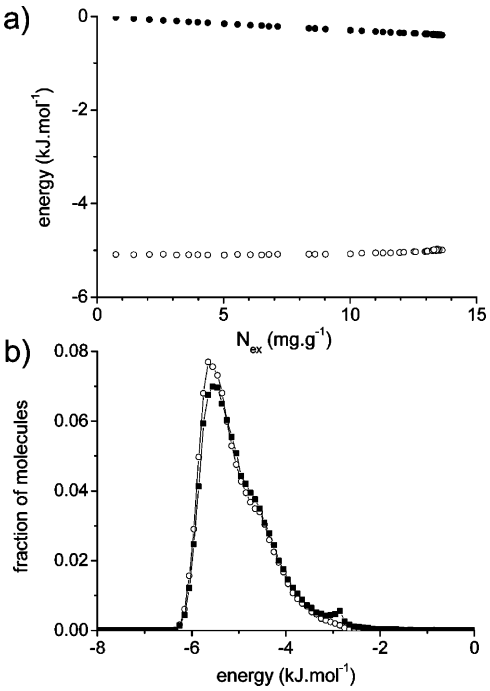

Figure 9. (a) Hydrogen−hydrogen potential energy (closed symbols) and hydrogen−**MIL-102** interactions (solid symbols) as a function of loading at 77 K. (b) Distribution of hydrogen/**MIL-102** interaction energies for individual hydrogen molecules at two different pressures (open symbols, 0.0025 MPa; closed symbols, 3.5 MPa).

the isosteric heat of adsorption would decrease with increasing loading, as the preferential low-energy sites are filled first at lower pressure.) The average value for the isosteric heat adsorption of ~6 kJ/mol is in line with experimentally measured values for hydrogen adsorption in other MOFs.[76] However, this value is far from the requirements for hydrogen storage (~15 kJ/mol).[77] A detailed analysis of the energetics is given in Figure 9a, where the total interaction is split into the hydrogen−framework and the hydrogen−hydrogen interactions. The hydrogen−**MIL-102** interaction is nearly constant over the whole range, further indicating that the material is energetically homogeneous. In contrast to this, the hydrogen−hydrogen interaction decreases with increasing loading. Additional evidence that **MIL-102** does not possess strong adsorption sites, which have been observed in other MOFs,[78,79] comes from Figure 9b, which shows a histogram of the interaction energy between individual hydrogen molecules and the **MIL-102** framework at two different pressures, 0.0025 and 3.5 MPa. In contrast to MOFs with larger pores and different adsorption sites—where the sites with the lowest interaction energy are occupied first and, at higher pressure, additional peaks for energetically less favorable sites emerge—the curves are nearly identical, showing a fairly narrow distribution. How restricted the pore space is for the hydrogen molecules in **MIL-102** is illustrated by the snapshot in Figure 10. Its free volume is only 26%, which is comparable to the free volume of microporous zeolites, such as silicalite,[80] but is considerably less than those observed for other MOFs, which can have free volume up to 90%. This is the main reason for the low hydrogen capacity of **MIL-102**, as the maximum amount adsorbed is proportional to the free volume.[81]

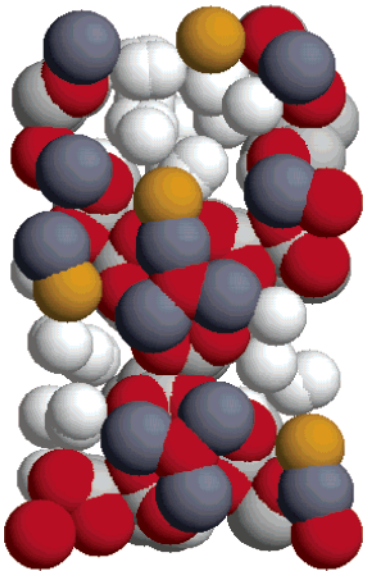

Figure 10. Snapshot of hydrogen adsorbed in **MIL-102** at 3.5 MPa.

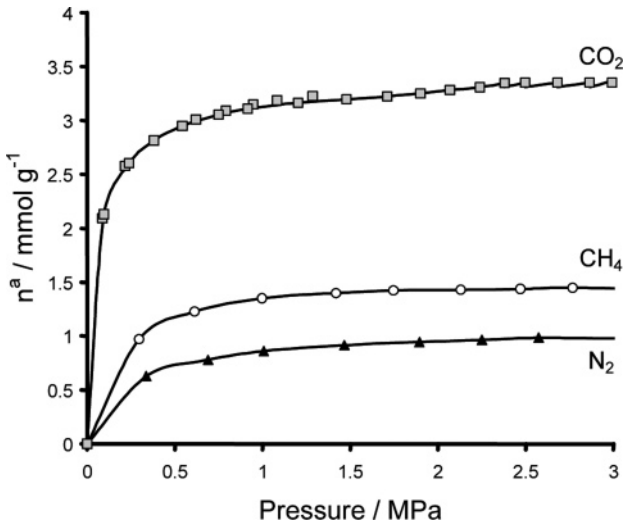

Figure 11. Isotherms of CO_2, CH_4, and N_2 on **MIL-102** at 304 K.

The experimental adsorption isotherms for carbon dioxide, methane, and nitrogen at 304 K are shown in Figure 11. This

(76) Rowsell, J. L. C.; Yaghi, O. M. *J. Am. Chem. Soc.* **2006**, *128*, 1304.
(77) Bhatia, S. K.; Myers, A. L. *Langmuir* **2006**, *22*, 1688.
(78) Spencer, E. C.; Howard, J. A. K.; McIntyre, G. J.; Rowsell, J. L. C.; Yaghi, O. M. *Chem. Commun.* **2006**, 278.
(79) Rowsell, J. L. C.; Spencer, E. C.; Eckert, J.; Howard, J. A. K.; Yaghi, O. M. *Science* **2005**, *309*, 1350.
(80) Düren, T.; Sarkisov, L.; Yaghi, O. M.; Snurr, R. Q. *Langmuir* **2004**, *20*, 2683.
(81) Frost, H.; Duren, T.; Snurr, R. Q. *J. Phys. Chem. B* **2006**, *110*, 9565.

shows that the adsorption of these gases occurs essentially below a pressure of 0.5 MPa, with no further significant adsorption up to 3.5 MPa. Such behavior is observed for small-pore zeolites, highlighting the relatively small pore opening of 4.4 Å, compared with 5.5 Å for silicalite. The total pore volume is relatively low compared to those of other MOF-type materials.[82] Nevertheless, the amount of CO_2 adsorbed in **MIL-102**, around 3.1 mmol·g^{-1} is similar to the value obtained with silicalite.[83] However, this quantity is far lower than that observed for other materials used in CO_2 recovery, such as NaX (5.4 mmol·g^{-1}) and Activated Carbon Maxsorb (22 mmol·g^{-1}).[84] The adsorption of methane and nitrogen is also quite limited, and again those values are similar to the ones observed for silicalite.[83] The adsorption of these gases is significantly lower than that of CO_2, as would be expected for physisorption phenomena where the higher the temperature, the less adsorption. This can sometimes be related to the ratio of the critical temperature to the experimental temperature (T_c/T_{exp}). In the present experiments, these values are around 0.4, 0.6, and 1 for N_2, CH_4, and CO_2, respectively. This corresponds well to the amounts of these gases adsorbed.

(82) Bourrelly, S.; Llewellyn, P. L.; Serre, C.; Millange, F.; Loiseau, T.; Férey, G. *J. Am. Chem. Soc.* **2005**, *127*, 13519.
(83) Dunne, J. A.; Mariwala, R.; Rao, M.; Sircar, S.; Gorte, R. J.; Myers, A. L. *Langmuir* **1998**, *12*, 5888.
(84) Himeno, S.; Komatsu, T.; Fujita, S. *J. Chem. Eng. Data* **2005**, *50*, 369.

Conclusion

MIL-102, or $Cr^{III}_3O(H_2O)_2F\{C_{10}H_4(CO_2)_4\}_{1.5}\cdot 6H_2O$, is a new example of a porous chromium carboxylate which exhibits several interesting features: (i) it has a trimeric inorganic subnetwork; (ii) it shows zeolitic behavior with no pore contraction; and (iii) it has a small hydrogen storage capacity of 1.0 wt % at 3.5 MPa and 77 K. Its adsorption behavior with respect to CO_2, CH_4, and N_2 at 304 K is similar to that of small-pore zeolites, such as silicalite. Other examinations are currently in progress and will be published soon.

JA064343U